Terrestrial gamma-ray flashes initiated by positive leaders

Joseph R. Dwyer
Department of Physics and Astronomy & Space Science Center (EOS), University of New Hampshire, Durham, New Hampshire 03824, USA

(Received 29 March 2021; accepted 9 June 2021; published 16 August 2021)

Terrestrial gamma-ray flashes (TGFs) are powerful submillisecond bursts of gamma rays produced by thunderstorms. To date, most TGFs have been observed by spacecraft in low-Earth orbit and have been found to be associated with negative intracloud lightning leaders. In recent years, TGFs have also been measured on the ground as downward beams originating from the overhead storms. While the majority of these ground-level TGFs appear to be associated with negative lightning leaders, similar to the TGFs seen from space, others are associated with upward-propagating positive leaders. In this paper, Runaway Electron Avalanche Model Monte Carlo simulations, modified to include low-energy electron and ion currents and self-consistent electric fields, are used to model TGF production by the relativistic feedback mechanism initiated by positive leaders. It is found that intense bursts of gamma rays are produced by positive leaders, similar to the observed ground-level TGFs. It is also found that these events produce dangerous radiation doses in excess of 1 Sievert and so may be of concern for aviation safety.

DOI: 10.1103/PhysRevD.104.043012

I. INTRODUCTION

Terrestrial gamma-ray flashes (TGFs) are highly luminous submillisecond bursts of gamma rays produced by thunderstorms [1]. Since their discovery in 1994, the vast majority of TGFs have been observed by spacecraft in low-Earth orbit [2–5]. For the TGFs in which lightning data are available, nearly all are associated with positive intracloud lightning and occur when the upward-propagating negative leader is about halfway between the negative and positive charge centers, suggesting that negative leaders are in some way linked to the production of these gamma-ray flashes [6].

In the last few years, a growing number of TGFs have been recorded by detectors on the ground near sea level, referred to here as ground-level TGFs, demonstrating that TGFs are not just produced in the upper parts of thunderstorms [7–14]. The majority of the ground-level TGFs are observed in association with downward propagating natural negative lightning [11–14]. However, other ground-level TGFs are clearly associated, not with negative leaders but with upward positive leaders (UPLs) [7–10]. These TGFs, which are remarkably bright, show properties surprisingly similar to those of the TGFs seen from space associated with negative leaders, including similar energy spectra, luminosities, durations, and smooth time-intensity profiles.

It is generally agreed that TGFs are produced by relativistic runaway electron avalanches (RREAs) accelerated in thunderstorm and/or lightning electric fields [15–18]. However, to produce a RREA, an energetic seed electron must be supplied to initiate the avalanche. Exactly how and where these seed electrons are generated is a key unanswered question that will be addressed in this work.

It is possible that TGFs are an extreme form of the x-ray emissions from lightning [19,20], with seed runaway electrons accelerated directly out of the low-energy free electron population in the high-field regions near leader tips and/or streamer heads [21–25]. However, it is not clear how this mechanism would apply to positive leaders, since the seeds would need to be created far from the leader tips in order to undergo the observed RREA multiplication.

Alternatively, when the amount of RREA multiplication is large, the relativistic feedback mechanism must be considered [22,26–29]. This mechanism involves the self-generation of energetic seed particles from backward-propagating positrons and back-scattered x rays. For the relativistic feedback mechanism to become self-sustaining, resulting in an exponential growth of RREAs, for each seed electron, the probability of generating a new seed electron must be greater than 1. This relativistic feedback threshold is reached for sufficiently large runaway electron avalanche multiplication factors, which generally occur for large electric fields and/or large potential differences.

As a lightning leader propagates, it greatly reduces the electric field along its hot channel and enhances the field in front of it, similar to a "snow plow" effect. For a large enough potential difference, the leader will inevitably cross the relativistic feedback threshold as long as the electric field in front of the leader exceeds the RREA threshold field $E_{th} = 267\ \mathrm{kV/m} \times n$, where n is the density of air relative to the International Standard Atmosphere (ISA)

value [26,30,31]. This condition seems likely, given that the RREA threshold field is lower than both the positive and negative streamer stability fields, thought to occur in the streamer zones of leaders [32]. As a result, relativistic feedback naturally explains TGFs produced in association with both negative and positive leaders.

II. PREVIOUS OBSERVATIONS

Here, we summarize two previous observations of ground-level TGFs produced in association with upward positive leaders made at the International Center for Lightning Research and Testing (ICLRT) at Camp Blanding, Florida. A third TGF, which occurred in Japan in association with a natural upward positive leader launched from a wind turbine, was so intense that all the detectors completely saturated and so will not be discussed further here [9,10].

The first ground-level TGF was observed during a rocket-triggered lightning flash in the summer of 2003 [7]. The downward TGF was detected during the initial stage in coincidence with a large initial, 10 kA, current pulse along the channel. At the time the TGF occurred, the upward positive leader, initiated by the rocket and wire, should have been several kilometers above the ground, approaching or entering the overhead thunderstorm. The TGF was very intense, saturating most NaI/photomultiplier tube detectors on the ground 600 m from the lightning channel. Figure 1 shows a histogram of greater than 1 MeV gamma rays recorded by one of the NaI(Tl)/photomultiplier tube (PMT) detectors [7]. The total duration of the recorded gamma-ray photons was approximately 300 μs, and the T_{90} duration was 170 μs, in the range of TGFs observed from space.

In 2014, a second TGF was observed at the ICLRT that was very similar to the 2003 event, again occurring during the initial stage of rocket-triggered lightning, in coincidence with a large current pulse (11 kA) along the channel [8]. Unlike the 2003 event, a Lightning Mapping Array

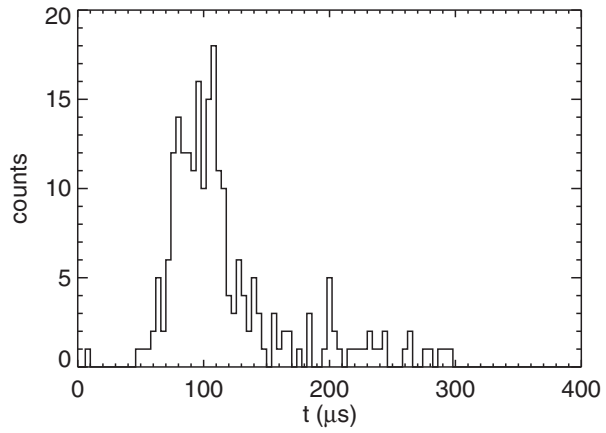

FIG. 1. Histogram of greater than 1 MeV gamma rays during the 2003 ground-level TGF as shown in Ref. [7].

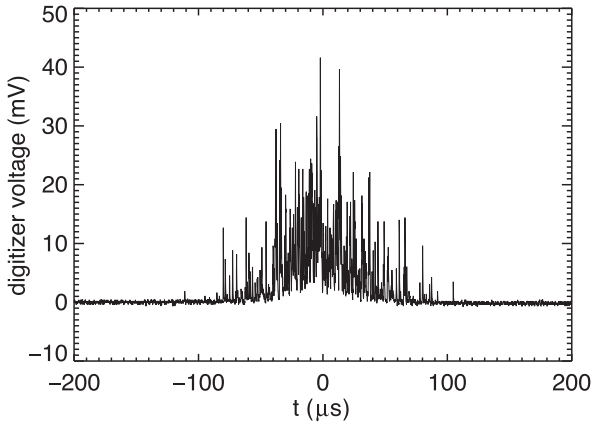

FIG. 2. Gamma-ray pulses recorded by a NaI(Tl)/PMT detector during the 2014 ground-level TGF [8].

(LMA) was operating near the ICLRT at the time, so the upward positive leader's location was observed. The TGF occurred when the leader reached an altitude of about 3.5 km. From the LMA data, there is no evidence for the presence of a downward negative leader occurring at the time of the upward positive leader associated with the 2014 ground-level TGF [8]. It is therefore assumed in this paper that the ground-level TGF was associated with the upward positive leader propagation. The existence of a downward negative leader during the 2003 ground-level TGF cannot be completely ruled out, since no LMA was operating then. However, the similarities between the 2003 and 2014 events suggest that a similar mechanism was involved.

The 2014 TGF had a fairly Gaussian pulse shape, with a full width at half maximum of 70 μs ($T_{90} = 120$ μs), that was quite smooth with no evidence of subpulses. Figure 2 shows gamma-ray pulses recorded by a NaI(Tl)/PMT detector [8]. The larger pulses seen in the plot are in the multi-MeV range. The fluence (greater than 50 keV) on the ground was 28 photons/cm^2 [33]. Depending on the orientation of the TGF and the beam geometry, Monte Carlo simulations show that at least 3.9×10^{15} gamma rays with energies greater than 1 MeV must have passed downward through a horizontal plane at 3.5 km, corresponding to a relativistic runaway electron grammage of 1.3×10^{17} g/cm^2 produced at the source [31]. Since this number is for a vertical narrow beam pointed directly at the detectors, the actual number of runaway electrons was likely much higher. For example, if the gamma rays were instead directed at a position on the ground 1 km from the detectors; then, an order of magnitude more runaway electrons and gamma rays would be required at the source.

III. SIMULATIONS

A. Particle simulations

The Runaway Electron Avalanche Model (REAM), used in this work, includes, in an accurate form, all the important

interactions involving runaway electrons, positrons, x rays, and gamma rays [26,27,28,31]. These interactions include energy losses through ionization and atomic excitation and Møller scattering. The simulation fully models elastic scattering using a shielded-Coulomb potential and includes bremsstrahlung production of x rays and gamma rays and the subsequent propagation of the photons, including Rayleigh scattering, Compton scattering, photoelectric absorption, and pair production. In addition, the simulation includes positron propagation (and annihilation) and the generation of energetic seed electrons via Bhabha scattering of positrons and Compton scattering, photoelectric absorption, and pair production of energetic photons. Results from REAM have appeared in many previous publications, including detailed comparisons with other Monte Carlo simulations including GEANT4 [34].

In previous versions of REAM, the energetic electrons and positrons were treated as test particles, propagating in specified electric and magnetic fields but not altering those fields. In the version presented in this work, the simulation is self-consistent, with the fields determining the particle motions and the particles altering the fields through the currents generated. After each time step, the runaway electrons are binned into cells using either cylindrical coordinates for cylindrically symmetric simulations (used in this work) or Cartesian coordinates for fully three-dimensional (3D) simulations. Because the simulation volume has dimensions of several kilometers, a variable grid size is used. For the simulation presented in this paper, the radial spacing of the grid points increases with the cylindrical radius from 3 m along the axis to 14 m at a radius of 500 m. The spacing in the z direction also varies, ranging from 3 m near the leader tip and in the streamer zone to 50 m along the leader channel.

The number of runaway electrons in each cell determines the amount of ionization generated in that time step, which is then used to determine the number densities of low-energy electrons and ions in each cell. This fully time dependent particle-in-cell method is especially useful for modeling relativistic feedback discharges, allowing the energetic particle production and propagation to be accurately modeled.

The goal of this work is to fully model terrestrial gamma-ray flashes, from start to finish. However, because TGFs are composed of about 10^{17} energetic particles, it is not possible to follow every electron, positron, or energetic photon. As a result, to keep the computation times manageable, the runaway electrons, positrons, and energetic photons are treated as "superparticles," with each particle carrying a weight to represent many other similar particles. This approach works especially well for RREAs, since as RREAs propagate and grow they become self-similar, having an approximately constant energy spectrum. As part of the development of the current code, the tests were performed to compare results with the previous, well-established version of the code to ensure that no biases were introduced, comparing energetic spectra, avalanche lengths, feedback factors, etc.

Simulations were started by injecting seed particles from a constant cosmic-ray background. As the lightning leaders propagate, the feedback factor increases, causing the seed particles to become almost entirely internally generated. The development of the TGF is then followed until the electric field partially collapses due to the large amount of ionization caused by the runaway elections, reducing the feedback factor below 1, and causing the injection of seed particles to fall again to the level from the cosmic-ray background.

B. Low-energy electrons and ions

The runaway electrons, positrons, and energetic photons are treated using the detailed Monte Carlo simulations. The low-energy (few eV) particles, including low-energy electrons, and positive and negative ions are not individually followed. Instead, the simulation volume is divided into cells, and the number densities of these low-energy particles are calculated for each cell. During the simulations, the low-energy electrons and ions only drift on the order of a few millimeters and centimeters, respectively, and since the cell sizes in the simulations are typically on the order of a few meters, changes in the densities due to the transport of low-energy particles are ignored. Instead, the currents in each cell are found as a function of time, and the charge in each cell is found from the currents using a finite volume method to ensure charge conservation, using the current densities at the cell boundaries to calculate the change in charge densities inside the cells.

During each time step, the density of runaway electrons, found from the REAM Monte Carlo simulation, determines the ionization rate in each cell according to

$$I = \alpha_{re}\nu_{re}n_{re}\ [\mathrm{m^{-3}\,s^{-1}}], \tag{1}$$

where $\alpha = 7860\ \mathrm{m^{-1}} \times n$ is the total number of low-energy (few eV) electrons and positive ions created per unit length by each runaway electron and n is the density of air relative to the ISA value. [35].

Most of the current generated by the relativistic feedback discharge is carried by the drifting low-energy electrons and the positive and negative ions. The current carried by the runaway electrons is small in comparison and is not included in the simulation. Within each cell, the densities change according to the following equations. These equations include the effects of impact ionization, two- and three-body attachment of the low-energy electrons, and ion-ion and ion-electron recombination,

$$\frac{dn_e}{dt} = \alpha_e n_e - \frac{n_e}{\tau_a} - \beta_e n_e n_+ + I, \tag{2}$$

$$\frac{dn_+}{dt} = \alpha_e n_e - \beta_i n_+ n_- - \beta_e n_+ n_e + I, \quad (3)$$

$$\frac{dn_-}{dt} = \frac{n_e}{\tau_a} - \beta_i n_- n_+, \quad (4)$$

where τ_a is the two- and three-body attachment time and α_e is the impact-ionization rate of the low-energy electrons, both of which are functions of the pressure and the electric field. The ion-ion and ion-electron recombination rates are $\beta_i = 1.0 \times 10^{-12}$ m^3/s and $\beta_e = 3.0 \times 10^{-13}$ m^3/s, respectively. [36–38]. The attachment of ions to cloud particles is important for time scales longer than about 10 ms and so plays a role in limiting the conductivity during gamma-ray glows but is negligible for TGF timescales. In this work, below 5 km altitude, the density of air is assumed to follow an exponential atmosphere with scale height of 10 km.

The current density from the drifting low-energy particles is

$$\vec{J}_{le} = -en_e\mu_e\vec{E} + en_+\mu_+\vec{E} - en_-\mu_-\vec{E}. \quad (5)$$

The drift velocities of the positive and negative ions in the electric field are found from $\vec{v}_\pm = \mu_\pm\vec{E}$, where $\mu_+ = (1.5 \times 10^{-4}$ m^2/Vs$)/n$ and $\mu_- = (-2.2 \times 10^{-4}$ m^2/Vs$)/n$ are the mobilities of the ion species, relative to ISA conditions, and $\vec{E}$ is the electric field vector [39]. The drift velocities of the low-energy electrons in the electric field are given by $\vec{v}_e = \mu_e\vec{E}$, where μ_e is the mobility of the electrons, which is sensitive to the electric field magnitude. At each location and time, the electron mobility, impact-ionization rate, and the two- and three-body electron attachment rates are found using data from Morrow and Lowke [40] and Liu and Pasko [41]. The total current density is the sum of the low-energy contribution and other currents, such as from thunderstorm charging and streamer zone currents (see below).

During the time step, dt, the change in the electric dipole moment density is

$$d\vec{P} = \vec{J}_{\text{tot}}dt. \quad (6)$$

The change in the charge density is

$$d\rho = -\vec{\nabla}\cdot d\vec{P}. \quad (7)$$

This total charge density is then calculated using Eq. (7), and the electric field is found.

C. Electric field

The electric potential is found by solving Poisson's equation, using the successive overrelaxation (SOR) technique with Chebyshev acceleration [42]. For each time step, the electric potential is calculated at the boundaries of the simulation volume by directly solving Coulomb's equation by integrating over the total charge density. For the present work, the potential at the ground is held fixed at $U = 0$, corresponding to an infinitely conductive ground plane.

The potential of the leader is held fixed at -1000 V/m, correspond to a highly conductive hot channel [43]. Current measurements made during the 2003 ground-level TGF show that the current along the channel exceeded 1 kA prior to the TGF. Once the boundary conditions are calculated, the SOR method calculates the potential from the total charge densities. The electric field vectors are then found by numerically calculating the gradient of the potential. The size of the time step is limited by the requirement that the maximum change in the electric field be small. Typical time steps are in the range of 10^{-8} to 10^{-9} s during the TGF.

For the simulations presented here, the initial electric field is calculated from planar charge regions, representing the main negative and lower positive charge layers, plus accompanying image charges from the conductive ground plane. The negative charge center is located at the top of the simulation volume above 4.4 km. This produces the electric field profile shown in Fig. 5 (right panel).

For the 3-D Cartesian coordinate case, an external magnetic field, such as the geomagnetic field, may be included. For cylindrically symmetric case, the internally generated, azimuthal magnetic fields are calculated from the electric currents using the Biot-Savart law. Although the simulations involve relativistic particles, the currents and charges are generated by nonrelativistic particles and vary relatively slowly with time, on the timescale of tens of microseconds, and so the electrostatic and magnetostatics approximations are justified for the cases presented in this work. Once the new electric and magnetic fields are calculated, the entire process described above is then repeated for the next time step. Also see Ref. [28] for more details.

D. Positive Leader propagation

The propagation of the upward positive leaders in the simulations are modeled by specifying the potential for the grid cells along the leader channel. For three-dimensional simulations, the channel can be specified to have a realistic branched structure. However, for the cylindrical symmetric cases presented in this work, the channel is vertical and located at the center of the cylindrical volume. The simulation starts with the leader channel near the ground and propagates upward with a velocity matching the LMA data for the upward positive leader associated with the 2014 ground-level TGF. The leader starts off very fast near the ground but slows down and is traveling at 1.0×10^5 m/s at the time of the TGF. The simulations that use this leader speed are called the slow leader cases. To see the dependence on the leader speed, a fast leader case is also included where the leader is moving at 5.0×10^5 m/s at the time of

the TGF. During the leader propagation, the conductivity on the channel is assumed to maintain a uniform channel electric field of −1000 V/m. Since the physics of the channel is not included in the simulation, for the work presented here, the finite impedance of the channel was ignored. The current flowing along the leader channel is calculated for each time step from the displacement current passing through the cylindrical surface of the leader channel.

E. Streamer zone

As the positive leader propagates, it reduces the electric field in its hot, conductive channel, enhancing the field in front of it. Current is fed into the channel by a large number of positive streamers initiated near the leader tip that propagate and branch in the streamer zone. For electric field strengths below the streamer propagation threshold field (i.e., the stability field), E_s, streamers may only travel a short distance before decaying. For fields above E_s, streamers will travel large distances, potentially branching multiple times, with larger currents produced by the streamers for larger fields above E_s. The threshold field for negative streamer propagation is about twice the value for positive streamer propagation, e.g., approximately 1000 and 500 kV/m at sea level, respectively. Following Bazelyan and Raizer [32], it is often assumed that the leader maintains a streamer zone field near E_s.

Although the physics of individual streamers is fairly well understood, most streamer simulations only follow streamers through a few centimeters of propagation with little or no branching. Because streamer zones may extend for many tens of meters, and likely involve a large amount of branching, streamer-streamer interactions, counter propagating streamers, and large changes to the electric field due to streamer currents, the physics of streamer zones is very complicated and so remains poorly understood. Indeed, it is not clear what electric field profiles exist in the streamer zones in front of leaders.

It is important to include streamer zone currents in front of the propagating leader, since without these currents the electric field in front of the propagating leader would quickly become unphysically large. Rather than attempting to develop a detailed model of the streamer zone, the accuracy of which would be questionable, in this work, a simple *ad hoc* model of the streamer zone conductivity is used, with the goal of capturing basic features of TGF production for a range of possible streamer zone configurations. In other words, individual streamers are not modeled. Instead, it is assumed that many streamers together create an average current density, which is zero below some threshold field, $E < E_{\text{thresh}}$, and increases exponentially above that value. Runaway electron avalanche lengths are typically several meters to hundreds of meters, and so the runaway electron physics is not sensitive to the small-scale structures of individual streamers, and so accurately modeling individual streamers is not necessary for this work.

In this paper, two streamer zone conductivity models are considered: a low-field case and a high-field case. The low-field case corresponds to a streamer zone field that is near the positive streamer stability field. In addition, a transition region where the streamers thermalize in front of the leader is included, further reducing the field near the leader tip. The conductivity in the thermalization region is assumed to fall off exponentially away from the leader tip. The conductivity is also assumed to grow exponentially with field strengths above the specified threshold field, assuming the streamer currents will be stronger as the electric field increases.

The high-field case corresponds to a streamer zone with the field near the negative streamer stability field. To see the results of a high field, no thermalization region was included in this case. The current densities used in the low-field and high-field cases are given by the equation

TABLE I. Properties of the simulated TGFs.

Case	E_{ave}/n [a] (kV/m)	Max E/n [b] (kV/m)	Leader speed [c] (m/s)	U_i [d] (MV)	U_{aval} [e] (MV)	N_γ [f]	RE grammage [g] (g/cm^2)	RMS [h] (μs)	T_{90} [i] (μs)	Peak current [j] (kA)	Max dose [k] (Sievert)
A	400	820	5.0×10^5	240	230	2.2×10^{17}	9.5×10^{18}	7.1	21	62	1.5
B	430	660	1.0×10^5	240	230	3.9×10^{16}	1.5×10^{18}	17	64	5.3	0.19
C	890	1400	1.0×10^5	150	130	1.2×10^{15}	8.4×10^{16}	30	96	1.1	0.047

[a]Average sea-level equivalent electric field in runaway electron avalanche region just before TGF.
[b]Maximum sea-level equivalent electric field in runaway electron avalanche region just before TGF.
[c]Leader speed at the time of the TGF
[d]Total potential difference between ground and cloud prior to leader propagation.
[e]Total potential difference in avalanche region just before TGF.
[f]Number of greater than 1 MeV gamma rays passing downward through a horizontal plane at 3.5 km altitude.
[g]Total path length of all runaway electrons multiplied by the local density of air (grammage).
[h]Root mean square of gamma-ray rate vs time as plotted in Fig. 5.
[i]T_{90} (time containing 90% of counts) of gamma-ray rate vs time as plotted in Fig. 5.
[j]Peak electric current injected into channel shown in Fig. 5.
[k]Maximum whole-body dose received by an individual inside an aircraft as plotted in Fig. 6.

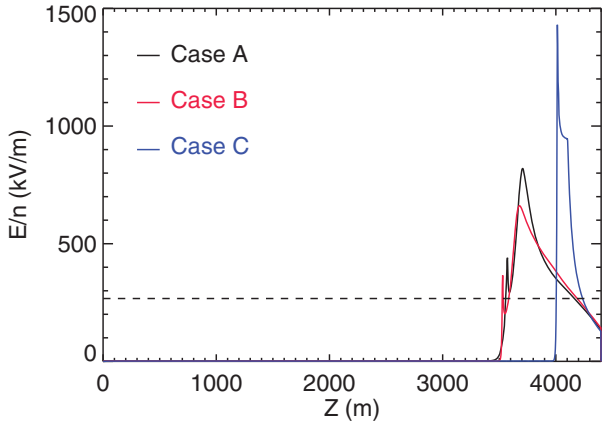

FIG. 3. Sea-level equivalent electric field along and above the leader channel versus altitude immediately before the TGFs for the three cases. The horizontal dashed line shows the RREA threshold field.

$$\vec{J}_S = \begin{cases} Ae^{-r/B}[e^{(E-E_{\text{thresh}})/C} - 1]\vec{E} & E > E_{\text{thresh}} \\ 0 & E \le E_{\text{thresh}} \end{cases}, \quad (8)$$

where the parameters in Eq. (8) are as follows: For the low-field case, the parameters are $E_{\text{thresh}} = 3.8 \times 10^5$ V/m $\times\, n$; $A = 4.43 \times 10^{-9}$ A/(Vm); $B = \infty$; $C = 2.0 \times 10^5$ V/m $\times\, n$. For the thermalization region (included in low-field case), the parameters are $E_{\text{thresh}} = 1.0 \times 10^5$ V/m $\times\, n$; $A = 8.85 \times 10^{-6}$ A/(Vm); $B = 15$ m; $C = 2.0 \times 10^5$ V/m $\times\, n$. For the high-field case, the parameters are $E_{\text{thresh}} = 9.4 \times 10^5$ V/m $\times\, n$; $A = 8.85 \times 10^{-7}$ A/(Vm); $B = \infty$; $C = 2.0 \times 10^5$ V/m $\times\, n$.

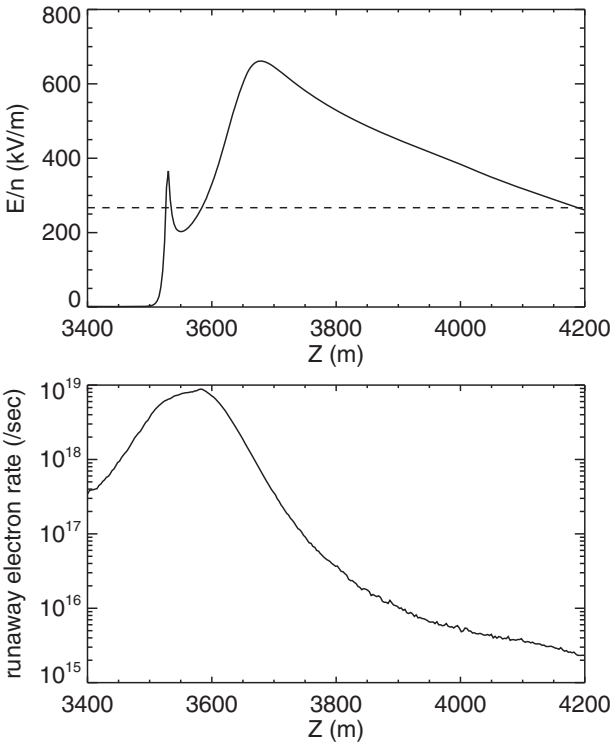

FIG. 4. Top: close-up of the sea-level equivalent electric field along and above the leader channel versus altitude immediately before the TGF for case B. The horizontal dashed line shows the RREA threshold field. Bottom: rate of runaway electrons passing downward through a horizontal plane versus altitude.

As an example, for the high-field case, an electric field 10% above the threshold field would relax back to the threshold field on a timescale on the order of several tens of microseconds. However, since the leader takes many milliseconds to move from the ground to the TGF source region, the field in front of the leader has time to settle into an approximately steady-state configuration.

In summary, in this paper, three simulations are presented (see Table I): a low-field, high-speed case (case A); a low-field, low-speed case (case B); and a high-field, low-speed case (case C).

Figure 3 shows the sea-level equivalent electric field along and above the leader channel versus altitude, for the three cases, after the feedback threshold is crossed and just before relativistic feedback partially discharges the high-field region in front of the leader. For case C, the feedback threshold is crossed at a higher altitude than for cases A and B because a lower total potential difference was used for that simulation. The increase in the field near the leader tip, e.g., seen near 3550 km in Fig. 4, occurs because for a given current through the streamer zone, as the field lines converge toward the leader tip, the current density must increase, requiring a large electric field to carry the current.

IV. RESULTS

A. TGF production

Figure 5 shows the electric field from the simulation for case A, immediately following the TGF. In the left panel, the leader channel is indicated by a narrow violet line in the center. The black lines with arrows show the average trajectories of the runaway electrons in the avalanche region. The dark volume in front of the leader tip has been partially discharged by the currents generated by the relativistic feedback discharge that produced the TGF. This discharged region is able to extend several hundred meters beyond the leader tip because a self-propagating relativistic feedback streamer is formed [28]. Because the relativistic feedback discharge reduces the electric field in the streamer zone in front of the leader channel, it is possible that the subsequent propagation of the leader will be affected.

The right panel shows the electric field along the central axis (black) and the initial electric field magnitude before the leader launched (initial field has plane symmetry). Case B has the same initial electric field as case A. For case C, the initial electric field profile is the same, but the maximum field is 0.62 times the value shown in Fig. 5.

The top panel in Fig. 6 shows the rate of greater than 1 MeV gamma rays passing downward through a horizontal plane at an altitude of 3.5 km. As can be seen, the two

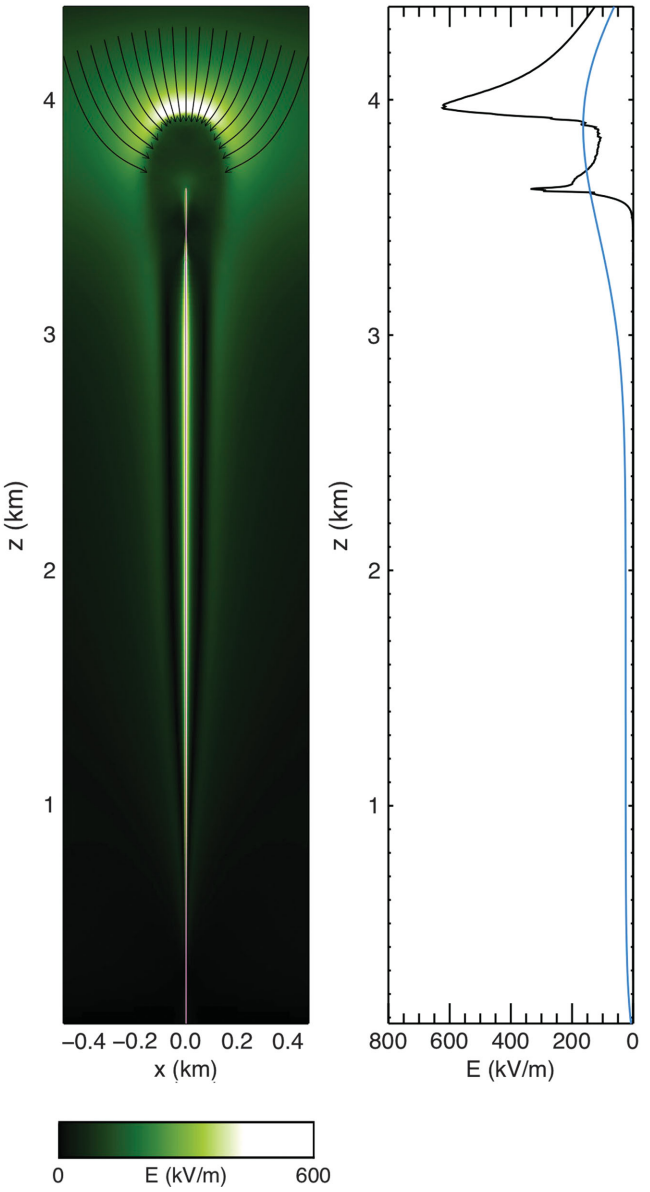

FIG. 5. Left: electric field strength produced by an upward positive leader that initiated a ground-level TGF. The leader channel is seen as the vertical purple line in the center. The black lines with arrows show the average trajectories of the runaway electrons. Right: electric field strength versus height immediately after the TGF (black) and prior to the lightning leader (blue).

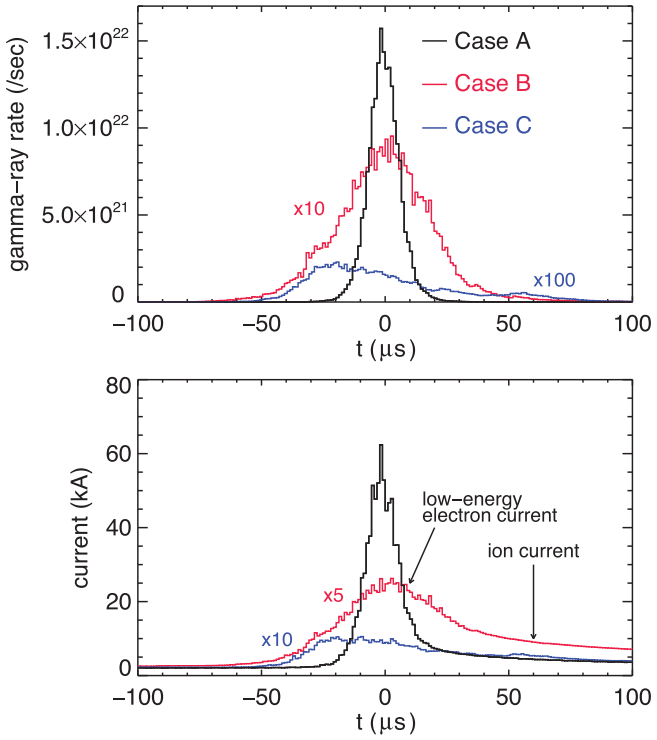

FIG. 6. Top: gamma-ray rate at 3.5 km vs time for the three simulated TGFs discussed in this paper. Bottom: electric currents injected into the top of the leader channel by the relativistic feedback discharge for the same three simulated TGFs.

low-E_s cases (cases A and B) produce roughly Gaussian time-intensity profiles, similar to the 2014 TGF. The high-E_s case (case C), in comparison, produces a more asymmetrical pulse with a long tail, which appears to be more consistent with the 2003 TGF. Table 1 lists properties of the three cases shown in Fig. 6. All three cases fall within the range of properties of TGFs detected from space and from the ground.

The bottom panel in Fig. 6 shows the electric current injected into the top of the lightning channel by the relativistic feedback discharge. Most of the runaway electrons produced during the relativistic feedback discharge travel toward the leader tip, generating large currents in the volume near the tip. These currents couple to the conducting leader channel, injecting current into the channel, which then propagates toward the ground.

The two main sources of current from the relativistic feedback discharge are current from the drifting low-energy electrons and current from the drifting positive and negative ions. The current from the runaway electrons is much smaller by at least an order of magnitude. Because the low-energy electrons undergo two- and three-body attachment to air on a timescale less than a microsecond, the current profile from the low-energy electrons closely matches the time-intensity profile of the runaway electrons that produce the ionization. Since the gamma rays are also directly produced by the runaway electrons, the low-energy electron current closely matches the TGF time profile as well, as is seen in Fig. 6 and as was reported by Dwyer *et al.* [7] and Hare *et al.* [8]. The ions are lost to ion-ion and ion-electron recombination and eventually attachment to cloud particles. However, these losses occur over much longer timescales, resulting in the long current tails seen in the bottom panel of Fig. 6.

The currents seen in Fig. 6 are quite large, comparable to return stroke currents. When these currents travel down the several-kilometer-long lightning channel, they will result in a large current moment on the order of a hundred kA-km,

producing a VLF-LF radio pulse, i.e. a "sferic," detectable at great distances.

B. Radiation doses

Runaway electrons are extremely penetrating and easily pass unimpeded through the walls of aircraft [24,44]. For TGFs associated with negative leaders, the runaway electrons travel away from the leader tip, potentially spreading out in the lower fields, thereby reducing the fluence and hence potential radiation doses. On the other hand, for TGFs associated with positive leaders, the runaway electrons travel toward the leader tip, focusing them into a small volume, producing a large fluence and a potentially dangerous radiation dose.

In Fig. 7, the whole-body radiation dose received by an individual inside an aircraft is plotted versus altitude for the three cases. Doses are found by multiplying the runaway electron fluences by 2.0×10^{-15} Sv m^2, found from Naval Research Laboratory SoftWare for Optimization of Radiation Detectors (SWORD) Monte Carlo simulations using a commercial jet mass model and a RREA input spectrum [45,46]. As can be seen, the radiation doses are dangerous over an extended region for all three cases, in some locations reaching levels that would likely induce radiation sickness. For case C, the radial electric field is large behind the leader tip, allowing runaway electrons to propagate behind the tip to the sides of the channel, creating the tail in the dose distribution seen in Fig. 7.

C. Threshold potential difference

Simulations show that the main factor in determining whether or not an upward positive leader will initiate a relativistic feedback discharge and hence a TGF is the total potential difference between the negative cloud charge and the ground. Earlier work on relativistic feedback discharges found the threshold potential difference versus electric field strength for a uniform field in a cylindrical volume

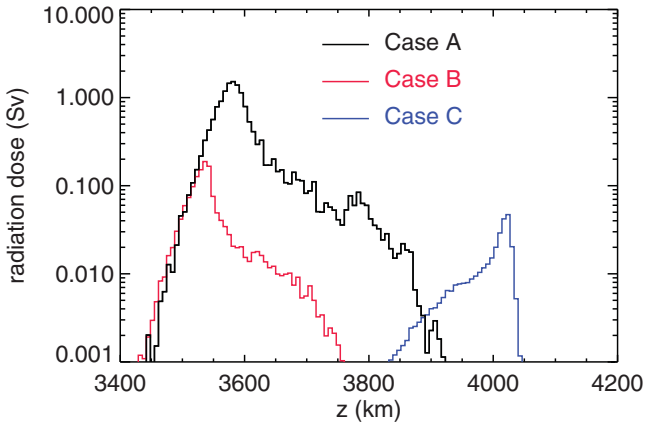

FIG. 7. Whole-body radiation dose received by an individual inside an aircraft vs attitude for the three simulated TGFs.

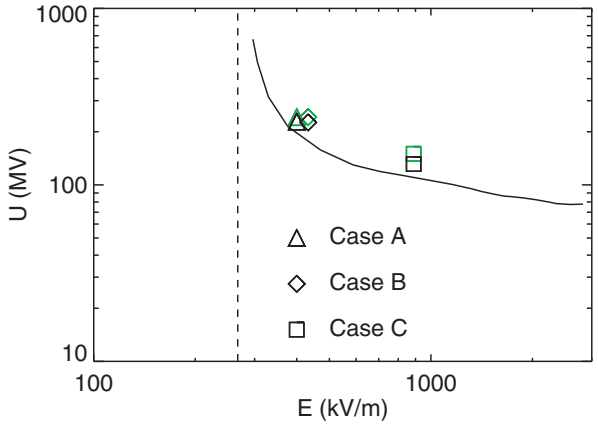

FIG. 8. Electric potential difference required to make a TGF vs the average ISA sea-level equivalent electric field inside the avalanche region. The solid curve is from REAM Monte Carlo simulations for a uniform field with limited lateral extent ($R = L/2$). The black symbols are potential differences in the avalanche region, and the green symbols are the total potential differences between the ground and the top of the simulation volume for the three simulated TGFs in this paper. The vertical dashed line is the RREA threshold field, E_{th}.

(radius = length/2) [27]. This threshold field is shown as the solid curve in Fig. 8. For the leaders modeled in this paper, the electric fields in front of the leaders are far from uniform. Nevertheless, as seen in Fig. 8, the potential difference versus the average electric field strength in the avalanche region for the three cases follows the estimation from the uniform field surprisingly well. For larger potential differences, simulations have found that TGFs with multiple pulses often result, since as the leader continues to propagate it may push the system above the relativistic feedback threshold again.

Approximately 250–300 upward positive leaders were generated during rocket-triggered lightning at the ICLRT from 2003 to 2014. During that same time period, two ground-level TGFs were recorded, implying that the fraction of UPLs that generate ground-level TGFs is about 1% [8]. This shows that ground-level TGFs, and possibly such large potential differences, are actually not that rare, especially considering the large amount of lightning in some locations.

V. CONCLUSIONS

In this paper, results of detailed Monte Carlo simulations of runaway electron and gamma-ray production in the high-field regions in front of positive lightning leaders are presented. Because the physics of energetic electrons, positrons, and gamma-rays are well known, the main uncertainties in the simulations are the electric currents in the streamer zones of the positive leaders, which translates into uncertainties in the electric fields in the streamer zones. Relativistic runaway electrons are mainly sensitive

to the large-scale fields, and so capturing the correct streamer microphysics is not necessary. Instead, three simple models were chosen to approximate the streamer zone fields with average fields near the positive and negative streamer stability fields and with low and high leader speeds.

All of these models were shown to produce TGF-like gamma-ray events with fluences on the ground, durations, and pulse shapes consistent with the observed ground-level TGFs. Choosing a different streamer zone field, i.e., a different form than for Eq. (8), may change some of the details of the gamma-ray emissions but should not change the basic conclusions of this paper: for a large enough potential difference, a relativistic feedback discharge, and hence a TGF, is the likely outcome of positive lightning leader propagation. While the focus of this paper has been on upward positive leaders from the ground, all the considerations of this work should also apply to positive leaders occurring during intracloud lightning. Indeed, it is possible that some of the TGFs observed from space and inferred to be associated with the negative leaders of the intracloud lightning may instead originate near the positive leader tips.

It is found that relativistic feedback discharges initiated from positive leaders may produce very large fluences of multi-MeV electrons, resulting in dangerous radiation doses to individuals inside aircraft at altitudes as low as a few kilometers. Given the number of aircraft struck by lightning each year, the risk posed by these TGF-producing discharges warrants further investigation.

ACKNOWLEDGMENTS

This research was supported in part by AFOSR Grant No. FA9550-16-1-0396. Any opinions, findings, and conclusions or recommendations expressed in this material are those of the authors and do not necessarily reflect the views of the Air Force Office of Scientific Research.

[1] J. R. Dwyer, D. Smith, and S. A. Cummer, High energy atmospheric physics: Terrestrial gamma-ray flashes and related phenomena, Space Sci. Rev., **133** (2012).
[2] D. M. Smith, L. I. Lopez, R. P. Lin, and C. P. Barrington-Leigh, Terrestrial gamma-ray flashes observed up to 20 MeV, Science **307**, 1085 (2005).
[3] M. S. Briggs *et al.*, A first results on terrestrial gamma ray flashes from the Fermi Gamma-ray Burst Monitor, J. Geophys. Res. **115**, A07323 (2010).
[4] M. Tavani *et al.* (AGILE Team) (2011), Terrestrial Gamma-Ray Flashes as Powerful Particle Accelerators, Phys. Rev. Lett. **106**, 018501 (2011).
[5] N. Østgaard, T. Neubert, V. Reglero, K. Ullaland, S. Yang, G. Genov *et al.*, First 10 months of TGF observations by ASIM, J. Geophys. Res. **124**, 14024 (2019).
[6] S. A. Cummer, F. Lyu, M. S. Briggs, G. Fitzpatrick, O. J. Roberts, and J. R. Dwyer, Lightning leader altitude progression in terrestrial gamma-ray flashes, Geophys. Res. Lett. **42**, 7792 (2015).
[7] J. R. Dwyer, M. A. Uman, H. K. Rassoul, V. A. Rakov, M. Al-Dayeh, E. L. Caraway, B. Wright, J. Jerauld, D. M. Jordan, K. J. Rambo, A. Chrest, and C. Smyth, A ground level gamma-ray burst observed in association with rocket-triggered lightning, Geophys. Res. Lett. **31**, L05119 (2004).
[8] B. M. Hare, M. A. Uman, J. R. Dwyer, D. M. Jordan, M. I. Biggerstaff, J. A. Caicedo, F. L. Carvalho, R. A. Wilkes, D. A. Kotovsky, W. R. Gamerota, J. T. Pilkey, T. K. Ngin, R. C. Moore, H. K. Rassoul, S. A. Cummer, J. E. Grove, A. Nag, D. P. Betten, and A. Bozarth, Ground-level observation of a terrestrial gamma ray flash initiated by a triggered lightning, J. Geophys. Res. **121**, 6511 (2016).
[9] G. S. Bowers, D. M. Smith, G. F. Martinez-McKinney, M. Kamogawa, S. A. Cummer, J. R. Dwyer, D. Wang, M. Stock, and Z. Kawasaki, Gamma ray signatures of neutrons from a terrestrial gamma ray flash, Geophys. Res. Lett. **44**, 10063 (2017).
[10] D. M. Smith, G. Bowers, M. Kamogawa, D. Wang, T. Ushio, J. Ortberg *et al.*, Characterizing upward lightning with and without a terrestrial gamma ray flash, J. Geophys. Res. **123**, 11321 (2018).
[11] Y. Wada, T. Enoto, K. Nakazawa, Y. Furuta, T. Yuasa, Y. Nakamura, T. Morimoto, T. Matsumoto, K. Makishima, and H. Tsuchiya, Downward Terrestrial Gamma-Ray Flash Observed in a Winter Thunderstorm, Phys. Rev. Lett. **123**, 061103 (2019).
[12] Y. Wada, T. Enoto, Y. Nakamura *et al.*, Gamma-ray glow preceding downward terrestrial gamma-ray flash, Commun. Phys. **2**, 67 (2019).
[13] Y. Wada, T. Enoto, Y. Nakamura, T. Morimoto, M. Sato, T. Ushio *et al.*, High peak-current lightning discharges associated with downward terrestrial gamma-ray flashes, J. Geophys. Res. **125**, e2019JD031730 (2020).
[14] R. U. Abbasi, T. Abu-Zayyad, M. Allen, E. Barcikowski, J. W. Belz, D. R. Bergman *et al.*, Gamma ray showers observed at ground level in coincidence with downward lightning leaders, J. Geophys. Res. **123**, 6864 (2018).
[15] J. R. Dwyer and D. M. Smith, A Comparison between Monte Carlo simulations of runaway breakdown and terrestrial gamma-ray flash observations, Geophys. Res. Lett. **32**, L22804 (2005).
[16] J. R. Dwyer and M. A. Uman, The physics of lightning, Phys. Rep. **534**, 147 (2014).
[17] A. V. Gurevich, G. M. Milikh, and R. A. Roussel-Dupré, Runaway electron mechanism of air breakdown and

preconditioning during a thunderstorm, Phys. Lett. A **165**, 463 (1992).
[18] N. G. Lehtinen, T. F. Bell, and U. S. Inan, Monte Carlo simulation of runaway MeV electron breakdown with application to red sprites and terrestrial gamma ray flashes, J. Geophys. Res. **104**, 24699 (1999).
[19] C. B. Moore, K. B. Eack, G. D. Aulich, and W. Rison, Energetic radiation associated with lightning stepped-leaders, Geophys. Res. Lett. **28**, 2141 (2001).
[20] J. R. Dwyer, M. A. Uman, H. K. Rassoul, M. Al-Dayeh, E. L. Caraway, J. Jerauld, V. A. Rakov, D. M. Jordan, K. J. Rambo, V. Corbin, and B. Wright, Energetic radiation produced during rocket-triggered lightning, Science **299**, 694 (2003).
[21] G. Moss, V. P. Pasko, N. Liu, and G. Veronis, Monte Carlo model for analysis of thermal runaway electrons in streamer tips in transient luminous events and streamer zones of lightning leaders, J. Geophys. Res. **111**, A02307 (2006).
[22] J. R. Dwyer, The source mechanisms of terrestrial gamma-ray flashes (TGFs), J. Geophys. Res. **113**, D10103 (2008).
[23] B. Carlson, N. Lehtinen, and U. Inan, Terrestrial gamma ray flash production by active lightning leader channels, J. Geophys. Res. **115**, A10324 (2010).
[24] J. R. Dwyer, D. M. Smith, M. A. Uman, Z. Saleh, B. Grefenstette, B. Hazelton, and H. K. Rassoul, Estimation of the fluence of high-energy electron bursts produced by thunderclouds and the resulting radiation doses received in aircraft, J. Geophys. Res. **115**, D012039 (2010).
[25] S. Celestin, W. Xu, and V. Pasko, Terrestrial gamma ray flashes with energies up to 100 MeV produced by non-equilibrium acceleration of electrons in lightning, J. Geophys. Res. **117**, A05315 (2012).
[26] J. R. Dwyer, A fundamental limit on electric fields in air, Geophys. Res. Lett. **30**, 2055 (2003).
[27] J. R. Dwyer, Relativistic breakdown in planetary atmospheres, Phys. Plasmas **14**, 042901 (2007).
[28] J. R. Dwyer, The relativistic feedback discharge model of terrestrial gamma ray flashes, J. Geophys. Res. **117**, A02308 (2012).
[29] A. B. Skeltved, N. Østgaard, B. Carlson, T. Gjesteland, and S. Celestin, Modeling the relativistic runaway electron avalanche and the feedback mechanism with GEANT4, J. Geophys. Res. **119**, 9174 (2014).
[30] L. P. Babich, E. N. Donskoy, R. I. Il'kaev, I. M. Kutsyk, and R. A. Roussel-Dupré, Fundamental parameters of a relativistic runway electron avalanche in air, Plasma Phys. Rep. **30**, 616 (2004).
[31] J. R. Dwyer, N. Liu, J. Eric Grove, H. Rassoul, and D. M. Smith, Characterizing the source properties of terrestrial gamma ray flashes, J. Geophys. Res. **122**, 8915 (2017).
[32] E. M. Bazelyan and Y. P. Raizer, *Spark Discharge* (CRC Press Boca Raton, FL, 1998).
[33] J. E. Grove, B. F. Phlips, E. A. Wulf, A. L. Hutcheson, L. J. Mitchell, R. S. Woolf, W. N. Johnson, M. M. Schaal, M. A. Uman, D. M. Jordan, B. Hare, J. R. Dwyer, H. Rassoul, and A. Bozarth, An intense terrestrial gamma-ray flash observed at ground level American Geophysical Union, in *Proceedings of the Fall Meeting 2015* (2015), abstract id. AE21A-04.
[34] D. Sarria, C. Rutjes, G.Diniz, A. Luque, K. M. A. Ihaddadene, J. R. Dwyer, N. Østgaard, A. B. Skeltved, I. S. Ferreira, and U. Ebert Evaluation of Monte Carlo tools for high-energy atmospheric physics II: relativistic runaway electron avalanches, Geosci. Model Dev. **11**, 4515 (2018).
[35] J. R. Dwyer and L. Babich, Low-energy electron production by relativistic runaway electron avalanches in air, J. Geophys. Res. **116**, A09301 (2011).
[36] S. McGowan, Ion-ion recombination in laboratory air, Phys. Med. Biol. **10**, 25 (1965).
[37] A. Franchin *et al.*, Experimental investigation of ion–ion recombination under atmospheric conditions, Atmos. Chem. Phys. **15**, 7203 (2015).
[38] F. L. Walls and G. H. Dunn, Measurement of total cross sections for electron recombination with NO^+ and O_2^+ using ion storage techniques, J. Geophys. Res. **79**, 1911 (1974).
[39] A. von Engel, *Ionized Gases*, 2nd ed. (Oxford University Press, New York, NY, 1965).
[40] R. Morrow and J. J. Lowke, Streamer propagation in air, J. Phys. D **30**, 614 (1997).
[41] N. Liu and V. P. Pasko, Effects of photoionization on propagation and branching of positive and negative streamers in sprites, J. Geophys. Res. **109**, A04301 (2004).
[42] W. H. Press, S. A. Teukolsky, W. T. Vetterling, and B. P. FlanneryNumerical Recipes in FORTRAN: The Art of Scientific Computing, 2nd ed. (Cambridge University Press, Cambridge, England, 1992).
[43] C. L. da Silva, R. G. Sonnenfeld, H. E. Edens, P. R. Krehbiel, M. G. Quick, and W. J. Koshak, The plasma nature of lightning channels and the resulting nonlinear resistance, J. Geophys. l Res. **124**, 9442 (2019).
[44] M. Pallu, S. Celestin, F. Trompier, and M. Klerlein, Estimation of radiation doses delivered by terrestrial gamma ray flashes within leader-based production models, J. Geophys. Res. **126**, e2020JD033907 (2021).
[45] C. S. Gwon, E. I. Novikova *et al.*, Interacting with the SWORD package (SoftWare for the Optimization of Radiation Detectors), IEEE Nucl. Sci. Symp. Conf. Rec. **2**, 1130 (2007).
[46] C. Gwon, J. Grove, J. R. Dwyer, K. Mattson, D. Polaski, and L. Jackson, Simulating terrestrial gamma-ray flashes using SWORD (Invited), *Proceedings of the Fall Meeting 2013, American Geophysical Union* (2013), abstract id. AE21A-02.